Rate constants for dissociative chemisorption of hydrogen molecules on copper clusters

R. C. Forrey*

Penn State University, Berks-Lehigh Valley College, Reading, Pennslyvania 19610-6009, USA

G. H. Guvelioglu, P. Ma, X. He, and H. Cheng[†]

Air Products and Chemicals, Inc., 7201 Hamilton Boulevard, Allentown, Pennsylvania 18195, USA

Transition state theory is used to estimate rate constants for dissociative chemisorption of H_2 on copper clusters. Activation energies and transition state partition functions are obtained from density functional theory for small clusters of less than 10 atoms. The violation of the Bronsted-Evans-Polanyi relation, which was previously observed for these clusters, is explained in terms of structural relaxation due to the chemisorption process. For large clusters, the impact of chemisorption on the global structure of the clusters is reduced. This restores the validity of the Bronsted-Evans-Polanyi relation and allows an extrapolation scheme for nano-size clusters to be developed.

PACS number(s): 68.43.Bc, 61.46.−w, 82.33.Hk, 82.65.+r

I. INTRODUCTION

Recent advances in nano-catalysis have identified transition metal (TM) clusters to be of fundamental importance.[1–6]. TM clusters constitute the majority of nano-catalysts used in contemporary homogeneous and heterogeneous catalytic systems.[7–10] Understanding chemical reactivity in small TM clusters is important for gaining insight into catalysis with larger clusters. The physicochemical properties of the clusters are strongly size-dependent. For example, chemically, gold nanoparticles can be highly reactive while gold bulk surfaces are very inert.[11–13] For many heterogeneous catalytic reactions, the catalysts are made in small nanoparticles dispersed on chemically inactive support materials and their efficiency is largely determined by the size and distribution of the nanoparticles on the supports.[14,15] Recent interest in gold-based catalysis has motivated theoretical studies of the chemical reactivity of O_2 and CO on unsupported Au clusters and surfaces.[16–18] It was later found that the supporting oxide materials also play an active role in the catalysis for gold-based systems.[19,20] Most theoretical studies on heterogeneous catalysis deal with chemical reactions on a crystalline surface, which provides valuable information on the properties of the catalysts at a scale much larger than the realistic catalysts. Unfortunately, fewer studies have been done for reactions on the catalyst nanoparticles themselves. The main difficulty arises from the fact that these particles are usually made of hundreds or thousands of atoms and their structures are essentially unknown; *ab initio* based quantum mechanical calculations on this scale of substance would be prohibitively expensive. Studies of chemical reactivity of small TM clusters at subnano scale, on the other hand, offer an alternative approach for gaining insight into the chemical reactivity of catalyst nanoparticles. By systematically searching for the lowest energy structures of the metal catalysts and their reactivity, one can obtain useful information on the evolution of physicochemical properties of the catalysts from subnano scale to bulk surface.

Recently, we began investigations of the evolution of small copper clusters and their chemical reactivity with molecular hydrogen.[21] The preferred sites for chemisorption were identified for clusters comprised of 2–15 atoms. Physicochemical properties were computed and compared with bulk and surface values. The results suggested that the binding energies of the most stable clusters increase smoothly with cluster size and approach an asymptote that is significantly less than the fcc bulk value. Therefore, the energy curves of the amorphous and crystalline growth paths must cross at a certain value of cluster size. This crossing point defines the location of a structure transition. Previous experimental studies[22,23] have shown that icosahedral structures are the most stable for cluster sizes ranging from 70 to 2500 atoms, whereas the pentagon bipyramid structure was found to be the most stable for small clusters.[21] Therefore, there may be multiple structure transitions in the evolution from small cluster to bulk, and it is unknown what influence such transitions might have on the chemical reactivity of the clusters as a function of cluster size. A detailed discussion and determination of the location of structure transitions for copper clusters is given in an accompanying paper.[24]

One of the objectives of this work is to provide estimates of rate constants where both experimental and theoretical data are lacking. This goal follows other efforts, such as the use of the empirical Bronsted-Evans-Polyani (BEP) relationship[25,26] or the reaction class transition state theory (TST) to provide estimates for a large number of reactions within a given class using knowledge of one or a few principal reactions.[27] In the present work, the principal reactions are hydrogen dissociative chemisorption onto small copper clusters. The rate constants are computed using conventional transition state theory with potential energy information computed using density functional theory (DFT). For small clusters, the chemisorption energies and activation barriers do not allow the use of the BEP relationship for estimating the transition state properties of one cluster from the properties of another cluster. This is due to significant relaxation that occurs in the structure of the cluster as a result of the chemisorption process. For larger clusters, the impact of chemisorption on the global structure is greatly reduced and only local relaxations near the chemisorption sites are ob-

served. This restores the validity of the BEP relation and allows extrapolation of activation barriers with cluster size. The extrapolation procedure does not take into account the transition to crystalline structure that occurs at large cluster size. Beyond the location of the crystalline structure transition, the rate constants should approach a limiting large cluster formula that may be derived from hydrogen chemisorption onto a crystalline copper surface. We provide comparisons of TST rate constants using extrapolations of small cluster data with those computed from the large cluster formula using experimental data for a bulk surface reaction. The estimated rate constants as a function of cluster size should provide input for computational fluid dynamics simulations that may prove useful for gaining a better understanding of nano-catalysis in TM clusters at the macroscopic scale.

II. THEORY

Within transition state theory, the dissociative chemisorption process for hydrogen molecules on a copper cluster of n atoms is given by

$$H_2(v,j) + Cu_n \rightarrow Cu_n H_2^{\ddagger}(i) \rightarrow Cu_n^* HH \quad (1)$$
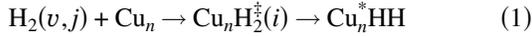
where v and j are the respective vibrational and rotational quantum numbers of the hydrogen molecule and i is the quantum number of the internal energy of the transition state cluster. A dagger $\ddagger$ is used to denote the transition state and an asterisk $*$ is used to denote an internally excited copper cluster, which is required to conserve total energy. The rate constant for the forward process (1) when averaged over the initial states is given by[28]

$$k_f(T) = \frac{k_B T}{h} \frac{Q_{H_2}^{\ddagger}}{Q_T Q_{H_2}} \exp(-E_0/k_B T) \quad (2)$$

where Q represents a partition function and E_0 is the threshold energy for the reaction at a temperature T. The activation energy is dominated by the threshold energy with small modifications arising from the temperature dependence of the partition functions. The exact Arrhenius activation energy is

$$E_a = E_0 - \frac{1}{2} k_B T + \langle E_{H_2}^{\ddagger} \rangle - \langle E_{H_2} \rangle \quad (3)$$

where $\langle E_{H_2}^{\ddagger} \rangle$ is the average internal energy of the cluster in the transition state and $\langle E_{H_2} \rangle$ is the average internal energy of the initial hydrogen molecule. The internal energies $E_{H_2}^{\ddagger}(i)$ may be computed from DFT electronic structure calculations. The threshold energy E_0 may be interpreted as the zero-point corrected potential energy barrier, which is also obtained in DFT calculations. Tunneling corrections may be included as modifications to the standard formulation (2). The simplest tunneling correction assumes a parabolic potential near the transition state[29] which results in the transmission coefficient

$$\kappa(T) = 1 + \frac{1}{24}(\hbar \omega^{\ddagger}/k_B T)^2 \quad (4)$$

where $\omega^{\ddagger}$ is the imaginary frequency at the transition state. The transmission coefficient (4) typically underestimates the

tunneling contribution as it accounts only for the region near the top of the barrier. A better approach is to use an Eckart correction or a more sophisticated variational transition state theory with a multidimensional tunneling correction.[30,31]

Transition state theory may also be used to describe the associative desorption process, which is the reverse of process (1). The rate constant is an inverse lifetime given by

$$k_b(T) = \frac{Q_{H_2}}{V} k_f(T) \exp(-E_b/k_B T) \quad (5)$$

where E_b is the chemisorption energy relative to the ground state of the hydrogen molecule and V is the volume of the cluster. Equation (5) was derived using detailed balance with the assumption that the energy distribution supplied by the cluster modes is Maxwellian. For desorption from a surface, it has been shown that a Gaussian distribution of excitation energy from the phonon bath leads to sticking coefficients of the form[32]

$$S_0(v,j,\theta,E_k,T) = \frac{A(v,j)}{2} \left[1 + \mathrm{erf}\left(\frac{E_k \cos^2 \theta - E_0(v,j)}{w(v,j,T)} \right) \right] \quad (6)$$

where S_0 is the zero-coverage sticking probability, $E_k = \frac{1}{2} m v^2$ is the translational kinetic energy, θ is the angle of the molecule with respect to the surface normal, and the parameters A, w, and E_0 all depend on the quantum state of the molecule. These parameters may also depend on the impact site and crystal orientation as well as the orientation of the molecule.

It is instructive to use the well-developed understanding of dissociative adsorption on surfaces for the H_2/Cu system to gain insight into the reactive behavior of H_2 in the presence of large Cu clusters. The largest amount of experimental data exists for the dissociative chemisorption of H_2 on Cu(111).[33–40] In the present work, we use the results of the IBM experiments[37] to evaluate the sticking probabilities defined by Eq. (6). The thermally averaged sticking rate coefficient per unit area for molecular bombardment onto a surface may be defined by[41]

$$k(T_g, T_s) = Q_{H_2}^{-1}(T_g) \sum_{v,j} g_j e^{-E_{vj}/k_B T_g} \int S_0(v,j,\theta,E_k,T_s)$$
$$\times [v \cos \theta] f(\vec{v}; T_g) \, d^3 \vec{v} \quad (7)$$

where T_g and T_s are the respective gas and surface temperatures, E_{vj} is the internal energy of the molecule, and f is the Maxwell-Boltzmann velocity distribution. The degeneracy factor g_j is equal to $\frac{1}{4}(2j+1)$ for even j and $\frac{3}{4}(2j+1)$ for odd j. For a large cluster, we assume that Eq. (7) may be integrated over the surface area of the cluster to obtain the rate constant. If we further assume that the cluster is spherical with a radius r and a temperature equal to that of the hydrogen gas, then Eq. (7) may be used to derive the large-r limit (LRL)

$$k_f(T) = \left(\frac{2\mu}{\pi h} \right) \left(\frac{\pi r^2}{Q_T Q_{H_2}} \right) \int_0^\infty e^{-E_k/k_B T} g(E_k) E_k \, dE_k \quad (8)$$

$$g(E_k) = \sum_{v,j} g_j e^{-E_{vj}/k_B T} \int_0^{\pi/2} S_0(v,j,\theta,E_k,T) \cos\theta \sin\theta \, d\theta$$

(9)

where the translational energy for the molecule-surface inter-action is replaced by $E_k = \frac{1}{2}\mu v^2$ with μ the reduced mass of the molecule-cluster system. The radius of the cluster may be estimated in terms of the copper density ρ and the number of atoms in the cluster

$$r \approx \left(\frac{3n}{4\pi\rho}\right)^{1/3} \approx 1.4 n^{1/3} \text{ Å}$$

(10)

This result shows that LRL rate constants scale as the cluster size to the two-thirds power. The TST results presented in the next section suggest that the forward rate constants are linear with cluster size. Therefore, there will be a crossing point where rate constants computed with the small cluster TST formula (2) using extrapolated DFT data intersect with those computed from the large cluster LRL formula (8) using ex-perimental data. It is unlikely that this crossing point coin-cides with the crossing point in the binding energy that de-fines the location of a structure transition. However, the change in behavior of the rate constants as more atoms are added is at least partially due to the change in structure that occurs as the cluster evolves from an amorphous to a crys-talline growth path.

III. RESULTS

Direct evaluation of potential energy barriers from quantum-mechanical calculations is computationally chal-lenging. Because transition states for multidimensional sys-tems are saddle points with a negative second derivative for motion along the reaction coordinate, a simple minimization procedure cannot be applied. Successful optimization of a transition state structure often requires a well-aligned initial structure that is sufficiently close to the true transition state structure. In the present work, the optimization was done by minimizing the norm of the force constants for each cluster. The calculation was performed using the linear synchronous transit (LST) method followed by the eigenvector following algorithm. Essentially, we started from the structures of re-actant ($Cu_n + H_2$) and the product ($Cu_n H_2$) to obtain a trial transition state structure by interpolating the reaction path-way using LST. The Hessian matrix was then calculated on the trial transition state geometry. We next performed a Newton-Raphson search on the potential energy surface, which searches for an energy maximum along one normal mode and a minimum along all other modes. The optimized transition state structure was confirmed by performing a nor-mal mode analysis that yielded an imaginary frequency with its normal mode pointing to the reactant and the product. The difficulty of such optimizations increases substantially with cluster size making it computationally impractical for large clusters. For this reason, we only performed transition state searches for copper clusters of up to 9 atoms. For larger clusters, we used the empirical BEP relation to obtain the energy barriers from the chemisorption energies.
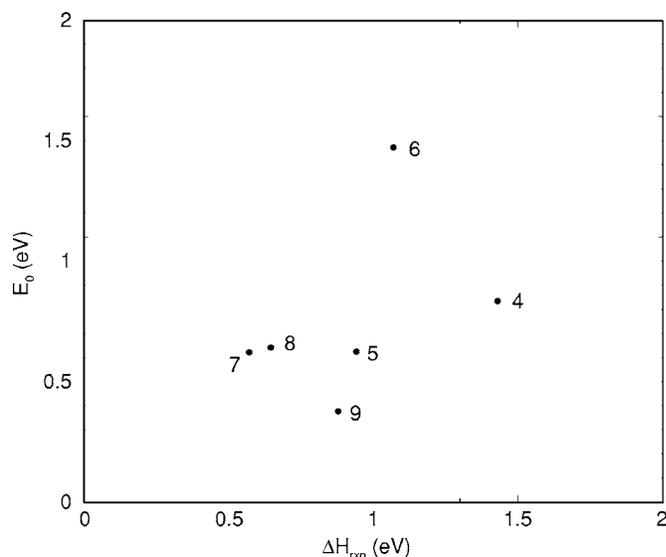

FIG. 1. Energy barrier vs heat of reaction. The data, which is labeled according to its cluster size, does not obey the linear Evans-Polyani relationship (Refs. 25 and 26) that typically exists between these two quantities. In the present context, the heat of reaction ΔH_{rxn} is assumed to be identical to the chemisorption energy E_b.

Figure 1 shows the energy barrier versus heat of reaction for cluster sizes 4–9. The data clearly violates the BEP rela-tion which states that there is a linear relationship between these two quantities. This violation is primarily due to $n=6$ and $n=9$. We have found that both of these clusters exhibit significant structural rearrangement upon chemisorption. Figure 2 demonstrates this point by comparing the minimum
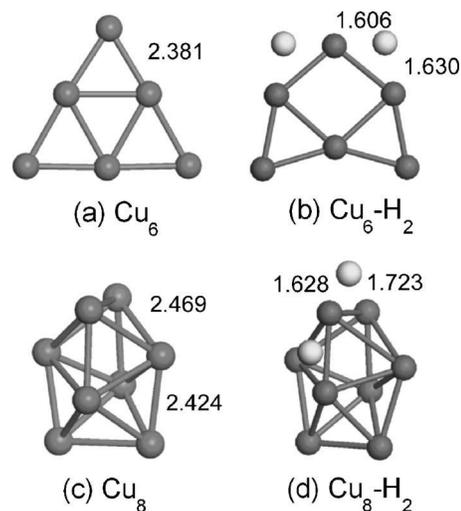

FIG. 2. Minimum energy structures for $n=6$ and $n=8$ clusters. The bare copper clusters are given in (a) and (c) and the clusters with chemisorbed hydrogen in (b) and (d). The global structural relaxation after chemisorption is much greater for $n=6$ than for $n=8$. The H atoms are highlighted and the bond lengths are given in angstroms. The base of the equilateral triangle shown at the top of (a) and its opposite angle increase by 51% and 63% respectively upon chemisorption, whereas the bond lengths and angles in (c) only change by about 8%.

TABLE I. Transition state energies (cm^{-1}).

Mode	$n=4$	$n=5$	$n=6$	$n=7$	$n=8$	$n=9$
1	37.3	44.0	20.1	71.8	63.3	58.7
2	109.6	75.0	36.4	76.9	93.0	65.3
3	162.6	109.5	50.4	93.8	96.3	77.1
4	187.5	125.3	102.0	123.6	101.8	85.5
5	215.5	154.7	120.5	128.1	108.9	95.2
6	231.6	190.8	140.8	133.9	114.3	102.2
7	301.5	217.1	165.0	137.9	115.2	105.3
8	388.0	227.9	184.8	152.3	118.4	108.7
9	1779.2	262.2	216.1	156.7	142.2	116.9
10	1839.7	316.5	228.6	163.2	155.3	130.4
11		402.2	275.4	193.2	156.3	136.7
12		1614.6	276.4	229.6	171.3	162.0
13		1882.1	323.0	232.7	172.4	165.3
14			1735.9	257.4	189.0	169.7
15			1824.3	1759.7	205.9	182.5
16				1779.2	211.3	191.0
17					218.9	204.3
18					234.3	208.9
19					303.0	223.6
20					1736.7	233.4
21					1866.9	268.2
22						325.4
23						519.5
24						1703.2
25						1781.9

energy structures for $n=6$ with $n=8$. The minimum energy structures for the two copper clusters are shown in Figs. 2(a) and 2(c) and for the clusters with chemisorbed hydrogen in Figs. 2(b) and 2(d). Whereas the $n=8$ cluster shows only small local bond deformations, the $n=6$ cluster shows global structural deformation after chemisorption. The $n=6$ and $n=9$ clusters exhibit the largest amount of structural relaxation which we believe is the reason for their large deviation from the linear BEP relationship. To test this hypothesis, we computed the energy of the bare $n=6$ copper cluster in the deformed configuration that exists after chemisorption. This energy is 0.462 eV higher than the minimum energy structure that was used as the reference energy in computing the barrier height and chemisorption energy. The effect of structural relaxation may be removed from the calculation by shifting the reference energy by 0.462 eV which yields $E_0 =1.009$ eV and $E_b=1.53$ eV. This pair of energies lies just above and to the right of the $n=4$ point of Fig. 1. When the structural relaxation is removed in this way, we get a good linear fit to the data with a slope of 0.25. As the cluster size increases above $n=10$, large global relaxation in the structure upon chemisorption is not observed. Therefore, we expect that the linear BEP relation obtained using rigid copper structures will be valid for large clusters.

Table I gives the positive energy eigenvalues of the transition state for the clusters. Several negative imaginary fre-

quencies were also found for each cluster. The lowest negative imaginary frequency, which corresponds to the hydrogen dissociative chemisorption pathway, has previously been reported for each cluster.[21] The additional frequencies may correspond to transition states on multiple reaction pathways, however, because they are very small it is more likely that they are a result of numerical noise. Table II gives the activation energies and rate constants for the clusters at three different temperatures. The activation energy defined by Eq. (3) is dominated by the barrier height obtained from the DFT calculations. The large variation in the rate constants is a consequence of the exponential dependence on the barrier height, which for small clusters is very sensitive to the cluster size. The Wigner transmission coefficients (4) are also given in Table II for each cluster size and temperature. The k_f data should be multiplied by κ to obtain the tunneling corrected rate constants. This will increase the 300 K results by about 1.5 times but have essentially no effect on the 900 K results. More sophisticated tunneling methods would presumably provide a stronger enhancement at low temperatures.

Table III gives estimates of the energy barriers and rate constants for clusters $n=10-15$. The BEP relation was used to compute the energy barriers from the chemisorption energies given in (Ref. 24). The energy barriers are less sensitive to cluster size with values ranging from 0.63 to 0.72 eV. The

TABLE II. Activation energies (eV) and rate constants (cm^3 s^{-1}).

	300 K			600 K			900 K		
n	E_a	k_f	κ	E_a	k_f	κ	E_a	k_f	κ
4	0.823	3.73×10^{-26}	1.59	0.787	2.14×10^{-19}	1.15	0.751	3.00×10^{-17}	1.07
5	0.612	1.81×10^{-22}	1.26	0.577	1.75×10^{-17}	1.06	0.539	6.26×10^{-16}	1.03
6	1.450	1.49×10^{-36}	1.64	1.420	1.72×10^{-24}	1.16	1.380	1.41×10^{-20}	1.07
7	0.611	3.01×10^{-22}	1.31	0.573	2.58×10^{-17}	1.08	0.535	8.79×10^{-16}	1.03
8	0.630	1.86×10^{-22}	1.32	0.592	2.36×10^{-17}	1.08	0.553	9.15×10^{-16}	1.04
9	0.363	6.25×10^{-18}	1.55	0.326	4.70×10^{-15}	1.14	0.288	3.32×10^{-14}	1.06

rate constants were computed from Eq. (2) using linear extrapolations for the transition state partition function as described below. When extrapolating to $n > 15$, we used a fixed energy barrier of 0.6 eV. This choice is based on the data in Table III, a computed value of 0.55 eV for the (111) face of an $n = 15$ cluster,[42] and the $n \to \infty$ surface value of 0.592 eV obtained from the IBM experiments.[37] With a fixed barrier height, the activation energy and rate constant will follow the cluster size dependency of the partition function $Q_{H_2}^{\ddagger}$.

For cluster sizes less than 10 atoms, $Q_{H_2}^{\ddagger}$ is approximately linear with n. This is shown in Fig. 3 for three different temperatures. The anomalous $n = 7$ data is likey a consequence of a higher zero-point energy compared to the other clusters (see Table I). The $n = 7$ cluster also represents the location of a structure transition from a two-dimensional triangular growth path to a three-dimensional pentagon bipyramid growth path.[21] Apart from the $n = 7$ data, the partition functions for the different growth paths appear to share the same linearity. The solid lines in Fig. 3 are linear best-fits to the DFT data. These fits, which will be used to extrapolate to larger cluster sizes, are given by

$$Q_{H_2}^{\ddagger}(300 \text{ K}) = 1.53n - 2.8$$

$$Q_{H_2}^{\ddagger}(600 \text{ K}) = 2.10n - 3.4$$

$$Q_{H_2}^{\ddagger}(900 \text{ K}) = 2.33n - 3.5 \tag{11}$$

The transition state partition function may be used to compute the average energy $\langle E_{H_2}^{\ddagger} \rangle$ of each cluster. Figure 4 shows $\langle E_{H_2}^{\ddagger} \rangle$ as a function of temperature for clusters 4–9. The average transition state energy provides an increasing contribution to the activation energy with temperature [see Eq. (3)].

However, the average energy of the H_2 molecule increases more strongly with T to produce an overall decrease in the activation energy. This temperature dependence is opposite to what was observed for copper surfaces.[37] As seen in Fig. 4, increasing the cluster size does not help to reconcile this difference. After an initial decrease with n, the curves seem to settle to approximately the same curve for $n > 6$. Therefore, the extrapolated $n \to \infty$ limit of the TST data does not lead to the measured results for the surface activation energy and it is better to use the LRL formulation.

Figures 5–7 show rate coefficients as a function of cluster size and temperature for different approximation schemes. In each plot, the threshold energy was taken to be either the fixed value of 0.6 eV or else the functional value $E_0(v, j)$ described below. The TST curves use Eq. (2) and generally give the smallest rate constants for each temperature when the cluster size is small. The LRL curves are shown for clusters with $n > 1000$. The curves labeled ARR use the simple Arrhenius function

$$k_f(T) = \pi r^2 \sqrt{\frac{8k_B T}{\pi \mu}} \exp(-E_0/k_B T) \tag{12}$$

where it is assumed that the energy barrier E_0 occurs at the radius r given by Eq. (10). This assumption, which was also used for the LRL curves defined by (8), generally produces rate constants that are significantly larger than those obtained using the partition function approach in transition state theory. This is partly due to using the bulk density for copper which assumes a lattice parameter of 3.61 Å. By contrast, we have found that the clusters $n = 2 - 15$ are slightly more dense with an average bond length of approximately 2.5 Å. Another reason for the relatively large LRL rate constants is the dependence of the threshold energy on the vibrational and

TABLE III. Energy barriers (eV) and rate constants (cm^3 s^{-1}).

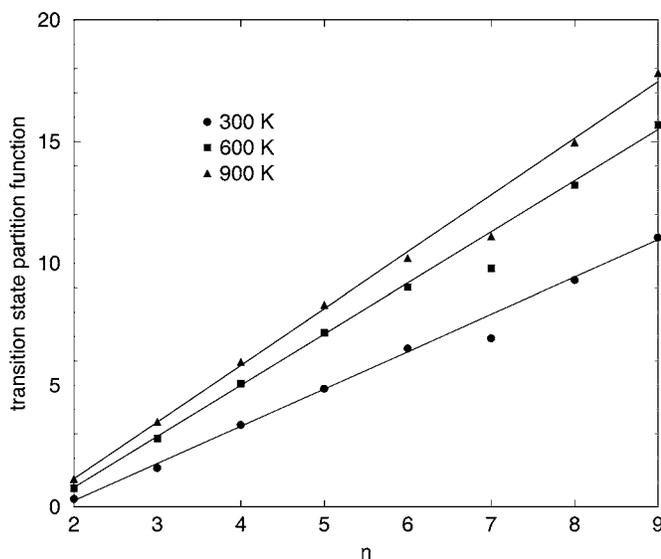| n	E_0	k_f (300 K)	k_f (600 K)	k_f (900 K)
10	0.71	1.73×10^{-23}	8.26×10^{-18}	4.96×10^{-16}
11	0.72	1.32×10^{-23}	7.62×10^{-18}	4.88×10^{-16}
12	0.65	2.19×10^{-22}	3.26×10^{-17}	1.33×10^{-15}
13	0.63	5.21×10^{-22}	5.26×10^{-17}	1.88×10^{-15}
14	0.66	1.78×10^{-22}	3.20×10^{-17}	1.39×10^{-15}
15	0.67	1.31×10^{-22}	2.85×10^{-17}	1.32×10^{-15}

FIG. 3. Transition state partition function versus cluster size. The linear fits to the computed data are given in Eq. (11). The anomalous points for $n=7$ are a consequence of the higher zero-point energy compared to the other clusters (see Table I).

rotational state of the hydrogen molecule. In Eq. (8), we used the experimental threshold energy[37]

$$E_0(0,j) = 0.592 + 0.0338j - 0.0079j^2 + 0.00022j^3$$

$$E_0(1,j) = 0.299 + 0.0200j - 0.00407j^2 \qquad (13)$$

to evaluate the sticking coefficient (6). For the TST1 curves, we used the constant value of 0.6 eV for the threshold energy. This difference is negligible for ground state molecules, however, there is a significant difference for the excited molecules that are populated by a thermal Boltzmann distribution. Therefore, an alternative calculation would be to use E_0 defined by (13) in Eq. (2) along with a Boltzmann average
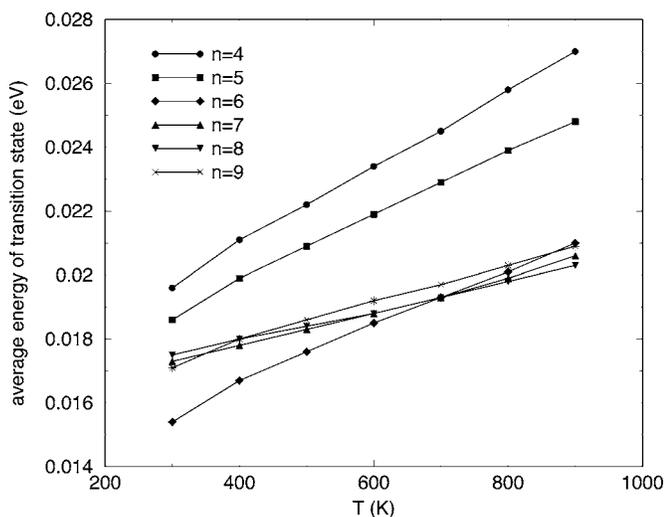

FIG. 4. Average transition state energy versus temperature. After an initial decrease with cluster size, the curves settle to approximately the same curve for $n > 6$.
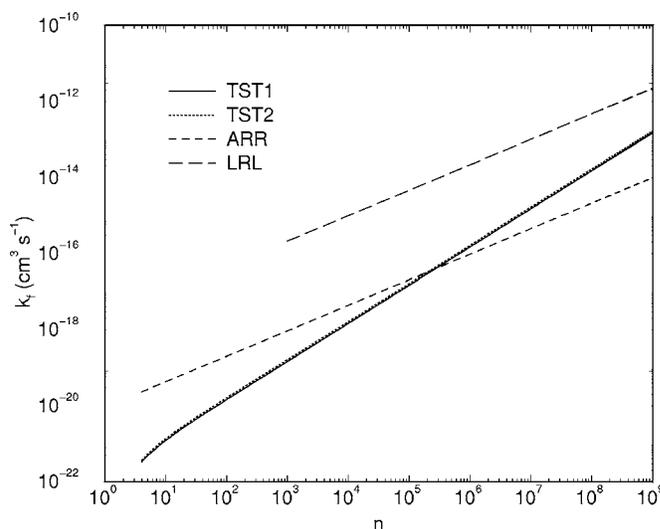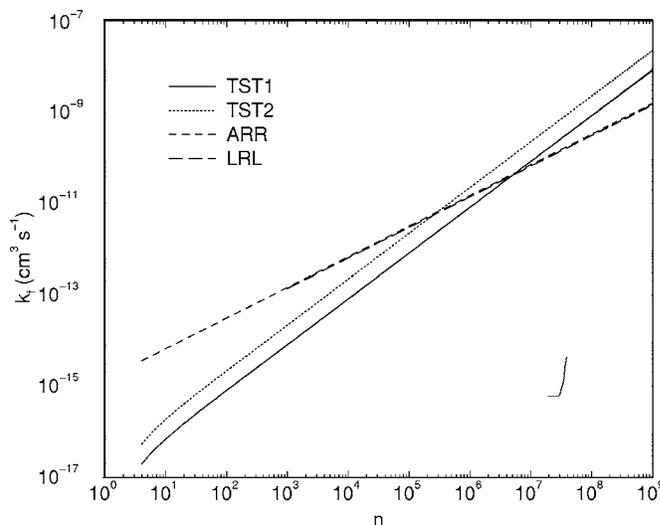

FIG. 5. Forward rate constants for $T=300$ K. The curves labeled TST1 and ARR use Eqs. (2) and (12) with $E_0=0.6$ eV to evaluate the rate constant. The curves labeled TST2 and LRL use Eqs. (2) and (8) with E_0 defined by (13) to evaluate the rate constants. There is little difference between the TST1 and TST2 curves for this temperature.

over the initial vibrational and rotational levels. The curves labeled TST2 in Figs. 5–7 include this calculation for the threshold energy. At 300 K, the hydrogen molecules are mostly in the ground state and the two TST curves do not differ appreciably. As the temperature is increased to 600 and 900 K, the TST2 curves are significantly higher than the TST1 curves.

As noted in Sec. II, the TST1 and TST2 curves increase linearly with n whereas the ARR and LRL curves increase as $n^{2/3}$. Therefore, the curves will intersect at large values of n.
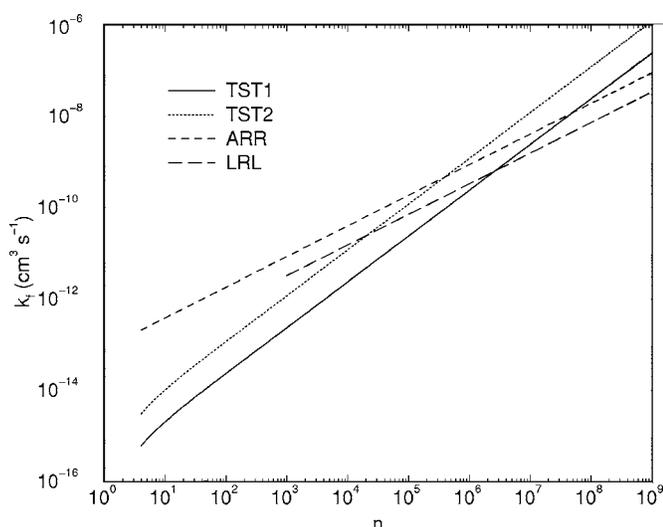

FIG. 6. Forward rate constants for $T=600$ K. The curves labeled TST1 and ARR use Eqs. (2) and (12) with $E_0=0.6$ eV to evaluate the rate constant. The curves labeled TST2 and LRL use Eqs. (2) and (8) with E_0 defined by (13) to evaluate the rate constants. There is little difference between the ARR and LRL curves for this temperature.

FIG. 7. Forward rate constants for $T=900$ K. The curves labeled TST1 and ARR use Eqs. (2) and (12) with $E_0=0.6$ eV to evaluate the rate constant. The curves labeled TST2 and LRL use Eqs. (2) and (8) with E_0 defined by (13) to evaluate the rate constants. All four curves are significantly different for this temperature.

At 300 K, there is little difference between the two TST curves which intersect with the ARR curve at a few hundred thousand atoms and the LRL curve at a few billion atoms. At 600 K, The ARR and LRL curves are nearly the same with intersection points around two hundred thousand atoms for TST2 and five million atoms for TST1. At 900 K, all four curves are significantly different from each other with intersection points ranging from twenty thousand to fifty million atoms. Due to structure transitions that are believed to occur at considerably smaller values of n,[24] it is unlikely that the crossover between the small cluster TST formulation and the large cluster LRL formulation would occur as shown in Figs. 5–7. All that can be reasonably predicted within the limitations of the present models are the small cluster results given by either of the TST curves and the large cluster results given by the LRL curves. Rate constants for intermediate size clusters ($n \sim 100$–10 000 atoms) probably fall in between the TST and LRL results, however, we have made no rigorous argument to support this speculation. The ARR results are shown for comparison and are presumably the least reliable of the estimates.

Figures 5–7 show that the LRL curves defined by Eq. (8) increase more slowly with temperature than the TST and Arrhenius curves defined by Eqs. (2) and (12). This is due to the increasing activation energy with temperature for the surface data compared to the decreasing activation energy for the TST data. This behavior is confirmed in Fig. 8, which shows the computed rate constant versus T^{-1} for $n=50$ along with linear best-fits. Because the vertical scale is logarithmic, the slope of the best-fit line may be interpreted as an average activation energy over the temperature range 300–900 K. Consistent with the IBM experiments,[37] we find that the LRL activation energy increases with T with an average value of 0.36 eV. The average activation energies for the TST1 and TST2 data over the same temperature range are 0.56 and 0.62 eV, respectively. The LRL data exhibits some curvature
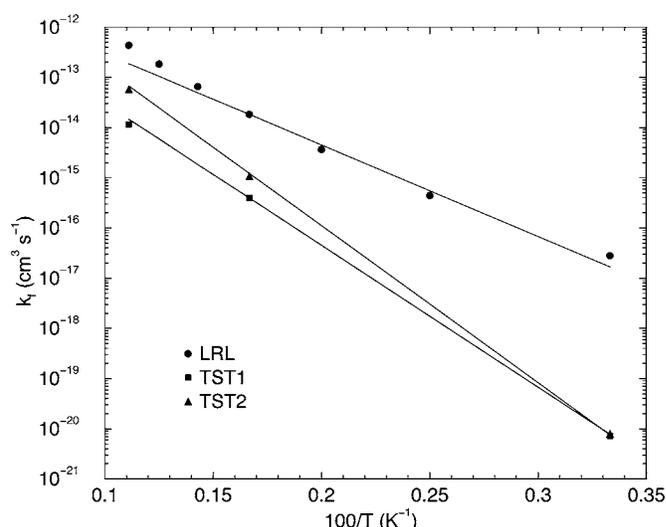

FIG. 8. Rate constants versus T^{-1} for $n=50$. The solid lines attempt to fit the data to a single activation energy. This works well for the TST data with average activation energies of 0.56 and 0.62 eV for $E_0=0.6$ eV and $E_0=E_0(v,j)$, respectively. The LRL data obtained from Eq. (8) is less linear with an average activation energy of 0.36 eV.

in Fig. 8 whereas the TST data is nearly linear over the full temperature range. This is because the LRL formulation accounts for tunneling through the width parameter w in Eq. (6) while the TST data has neglected tunneling. In future applications, it would be desirable to improve the TST data by using more sophisticated tunneling methods.

Figure 9 shows the rate coefficient for the backward associative desorption reaction as a function of cluster size. Here, we have used Eq. (5) together with DFT results for the chemisorption energy that may be fit to the formula
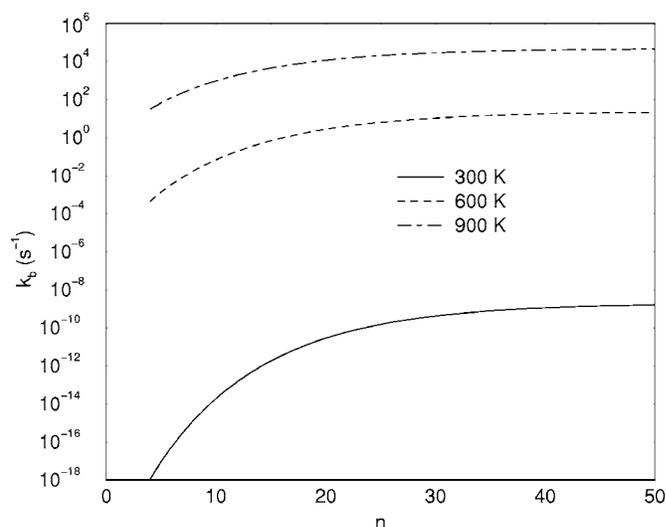

FIG. 9. Backward rate constant vs cluster size. The results were computed using Eqs. (5) and (14) with TST1 data for the forward rate constants. The curves reach a constant large-n asymptote for all temperatures.

$$E_b = E_\infty + A\exp(-Bn) \qquad (14)$$

where $A = 0.8$ eV, $B = 0.1$, and $E_\infty = 0.6$ eV. Because the forward rate constant (2) is linear with n, the pre-exponential factor of the backward rate constant (5) does not depend on the cluster size. Therefore, the n-dependence of k_b will be controlled by the chemisorption energy. For large-n, the formula (14) shows that the chemisorption energy quickly approaches the bulk result E_∞. This requires k_b to approach a constant value as n increases. Figure 9 shows results for three temperatures using TST1 data for the forward rate constants. The differences between the three curves is larger than for the forward direction due to the increased effective barrier $E_0 + E_b$. Similar results were found using TST2 data. The LRL formulation should not be used with Eq. (5) because the detailed balance formula was derived using a forward rate constant defined by Eq. (2). However, if the LRL forward rate constant (8) is naively substituted into Eq. (5), then the backward rate constant k_b would initially increase and flatten out as in Fig. 9, before eventually decreasing as the minus one-third power of the cluster size.

IV. CONCLUSIONS

We have presented estimates of rate constants for dissociative chemisorption of H_2 on copper clusters. Using detailed balance together with chemisorption energies, we have also estimated rate constants for the reverse process of associative desorption. Our calculations use conventional transition state theory with potential energy information obtained from density functional theory. For small clusters, we have provided benchmark results that are extremely sensitive to cluster size. We have shown that this sensitivity is due to structural rearrangements that occur as a result of the chemisorption process prohibiting the use of the BEP relation when $n < 10$. For $n \geq 10$, the structural relaxations are local and the utility of the BEP relation is restored. Using calculated chemisorption energies for $10 \leq n \leq 15$, we applied the BEP relation to estimate the energy barriers and rate constants. The sensitivity of the energy barriers to cluster size is significantly reduced as $n \to \infty$ allowing the development of an extrapolation scheme for large clusters. This extrapolation scheme uses a fixed energy threshold and a linear fit to the partition function of the transition state molecule. The extrapolations do not appear to be sensitive to the differences in growth path that govern the evolution of small clusters. As the clusters grow larger in size, they must undergo a transition to crystalline structure. Therefore, we expect the rate constants to reflect this change in structure and approach a limiting large cluster formula that we have derived from hydrogen chemisorption onto a crystalline copper surface. We have provided comparisons of the extrapolated TST rate constants with the large cluster formula.

Qualitative and semiquantitative descriptions of kinetics for chemisorption on TM nanoparticles are important for understanding heterogeneous catalysis for many systems. Computationally, it becomes increasingly difficult to evaluate the activation barrier for the chemisorption process as the size of the metal clusters increases. In addition, significant uncertainties associated with the electronic structure methods for evaluation of transition state energies further prohibits an accurate description of the kinetics. Therefore, the results presented here are not expected to be of high accuracy, particularly in the region near a structure transition. Instead they attempt to address the question of how to estimate rate coefficients for chemical reactions that occur on the surface of clusters of varying size. It is hoped that these results will motivate experimental investigations on this issue. The results also serve as a starting point for computational fluid dynamics simulations[43] that may prove useful for gaining a better understanding of nano-catalysis in transition metal clusters.

---

*Corresponding author. Electronic address: rcf6@psu.edu

†Corresponding author. Electronic address: chengh@airproducts.com

[1] H. Cheng and L. S. Wang, Phys. Rev. Lett. **77**, 51 (1996).

[2] L. S. Wang, H. Wu, and H. Cheng, Phys. Rev. B **55**, 12884 (1997).

[3] D. P. Pappas, A. P. Popov, A. N. Anisimov, B. V. Reddy, and S. N. Khanna, Phys. Rev. Lett. **76**, 4332 (1996).

[4] K. Lee, J. Callaway, and S. Dhar, Phys. Rev. B **30**, 1724 (1984).

[5] K. Lee, J. Callaway, K. Kwong, R. Tang, and A. Ziegler, Phys. Rev. B **31**, 1796 (1985).

[6] M. Castro and D. R. Salahub, Phys. Rev. B **49**, 11842 (1984).

[7] R. Whyman, in *Transition Metal Clusters*, edited by B. F. G. Johnson (Wiley, New York, 1980).

[8] E. L. Muetterties, Science **196**, 839 (1977).

[9] H. Conrad, G. Ertl, H. Knozinger, J. Kuppers, and E. E. Latta, Chem. Phys. Lett. **42**, 115 (1976).

[10] H. Haberlandt, in *Theoretical Aspects of Heterogeneous Catalysis*, edited by J. B. Moffat (Van Nostrand Reinhold, New York, 1990).

[11] B. Hammer and J. K. Norskov, Nature (London) **376**, 238 (1995).

[12] M. Haruta, Catal. Today **36**, 153 (1997).

[13] M. Valden, X. Lai, and D. W. Goodman, Science **281**, 1647 (1998).

[14] C. R. Henry, Surf. Sci. Rep. **31**, 235 (1998).

[15] U. Heiz, A. Sanchez, S. Abbet, and W.-D. Schneider, Chem. Phys. **262**, 189 (2000).

[16] M. Mavrikakis, P. Stoltze, and J. K. Norskov, Catal. Lett. **64**, 101 (2000).

[17] G. Mills, M. S. Gordon, and H. Meitu, Chem. Phys. Lett. **359**,

493 (2002).

[18] Z.-P. Liu, P. Hu, and A. Alavi, J. Am. Chem. Soc. **124**, 14770 (2002).

[19] L. M. Molina and B. Hammer, Phys. Rev. Lett. **90**, 206102 (2003).

[20] Z.-P. Liu, X.-Q. Gong, J. Kohanoff, C. Sanchez, and P. Hu, Phys. Rev. Lett. **91**, 266102 (2003).

[21] G. H. Guvelioglu, P. Ma, X. He, R. C. Forrey, and H. Cheng, Phys. Rev. Lett. **94**, 026103 (2005).

[22] B. J. Winter, E. K. Parks, and S. J. Riley, J. Chem. Phys. **94**, 8618 (1991).

[23] D. Reinhard, B. D. Hall, P. Berthoud, S. Valkealahti, and R. Monot, Phys. Rev. Lett. **79**, 1459 (1997).

[24] G. H. Guvelioglu, P. Ma, X. He, R. C. Forrey, and H. Cheng, preceding paper, Phys. Rev. B **73**, 155436 (2006).

[25] N. Bronsted, Chem. Rev. (Washington, D.C.) **5**, 231 (1928).

[26] M. G. Evans and N. P. Polanyi, Trans. Faraday Soc. **34**, 11 (1938).

[27] T. N. Truong, J. Chem. Phys. **113**, 4957 (2000).

[28] R. D. Levine and R. B. Bernstein, *Molecular Reaction Dynamics and Chemical Reactivity* (Oxford University Press, New York, 1987).

[29] E. Wigner, J. Chem. Phys. **5**, 720 (1937).

[30] T. N. Truong, D. K. Maity, and T. T. Truong, J. Chem. Phys. **112**, 24 (2000).

[31] W. T. Duncan, R. L. Bell, and T. N. Truong, J. Comput. Chem. **19**, 1039 (1998).

[32] A. C. Luntz, J. Chem. Phys. **113**, 6901 (2000).

[33] H. A. Michelsen and D. J. Auerbach, J. Chem. Phys. **94**, 7502 (1991).

[34] C. T. Rettner, D. J. Auerbach, and H. A. Michelsen, Phys. Rev. Lett. **68**, 1164 (1992).

[35] H. A. Michelsen, C. T. Rettner, and D. J. Auerbach, Phys. Rev. Lett. **69**, 2678 (1992).

[36] H. A. Michelsen, C. T. Rettner, D. J. Auerbach, and R. N. Zare, J. Chem. Phys. **98**, 8294 (1993).

[37] C. T. Rettner, H. A. Michelsen, and D. J. Auerbach, J. Chem. Phys. **102**, 4625 (1995).

[38] D. Wetzig, M. Rutkowski, R. David, and H. Zacharias, Europhys. Lett. **36**, 31 (1996).

[39] H. Hou, S. J. Gulding, C. T. Rettner, A. M. Wodtke, and D. J. Auerbach, Science **277**, 80 (1997).

[40] M. J. Murphy and A. Hodgson, J. Chem. Phys. **108**, 4199 (1998).

[41] R. K. Pathria, *Statistical Mechanics* (Pergamon, New York, 1972).

[42] J. E. Müller, Surf. Sci. **272**, 45 (1992).

[43] X. He, N. Li, and B. Goldstein, Mol. Simul. **25**, 145 (2000).